JACS JOURNAL OF THE AMERICAN CHEMICAL SOCIETY
Communication
Cite This: J. Am. Chem. Soc. 2019, 141, 13330−13335
pubs.acs.org/JACS

A Synthetic Model of Enzymatic $[Fe_4S_4]$−Alkyl Intermediates

Mengshan Ye, Niklas B. Thompson, Alexandra C. Brown, and Daniel L. M. Suess*

Department of Chemistry, Massachusetts Institute of Technology, Cambridge, Massachusetts 02139, United States

Supporting Information

ABSTRACT: Although alkyl complexes of $[Fe_4S_4]$ clusters have been invoked as intermediates in a number of enzymatic reactions, obtaining a detailed understanding of their reactivity patterns and electronic structures has been difficult owing to their transient nature. To address this challenge, we herein report the synthesis and characterization of a 3:1 site-differentiated $[Fe_4S_4]^{2+}$−alkyl cluster. Whereas $[Fe_4S_4]^{2+}$ clusters typically exhibit pairwise delocalized electronic structures in which each Fe has a formal valence of 2.5+, Mössbauer spectroscopic and computational studies suggest that the highly electron-releasing alkyl group partially localizes the charge distribution within the cubane, an effect that has not been previously observed in tetrahedrally coordinated $[Fe_4S_4]$ clusters.

Iron−sulfur (Fe−S) proteins are found in all kingdoms of life and perform myriad functions in the cell.[1−4] Those that utilize $[Fe_4S_4]$ cofactors are the most ubiquitous and have well-documented roles as electron-transfer and Lewis acid catalysts.[1,2] Recently, several classes of $[Fe_4S_4]$ enzymes have been proposed to operate via organometallic intermediates. In particular, $[Fe_4S_4]$−alkyl species have been invoked in mechanisms of reductive dehydroxylation reactions in isoprenoid biosynthesis,[5−11] reductive coupling of CO and CO_2 to higher-order hydrocarbons,[12] and radical reactions by the >100 000 members of the radical *S*-adenosyl-L-methionine (SAM) superfamily of enzymes.[13−16]

Despite the emerging significance of $[Fe_4S_4]$−alkyl intermediates, little is known about how these species form, their reactivity patterns, or their electronic structures. Moreover, no $[Fe_4S_4]$−alkyl species have been structurally characterized and their identification as intermediates (Chart 1) has relied on EPR/ENDOR[5−11,13−15] or DFT[7,12] studies. And although reliable models for the electronic structures of $[Fe_4S_4]$ clusters have been developed,[17−19] these models were derived for clusters ligated by relatively weak-field, moderately donating ligands (e.g., cysteine thiolates). How binding of a strong-field, highly electron-releasing alkyl ligand[20] perturbs the electronic structure of $[Fe_4S_4]$ clusters—to what extent it induces valence localization, how (if at all) it affects Fe−Fe interactions, and how these effects impact the reactivity of the Fe−C bond—is unknown.

Synthetic chemistry will play an important role in answering these questions. Synthetic analogues of $[Fe_4S_4]$−alkyl intermediates would, for example, allow for the structures of intermediates to be elucidated (by linking their structures with their spectroscopic features) and for their electronic structures to be interrogated. These efforts are hampered by the lack of synthetic access to alkylated $[Fe_4S_4]$ clusters. To date, only one alkylated Fe−S cluster has been structurally characterized—an $[Fe_8S_7]$ cluster in which the alkyl group is derived from decamethylcobaltocene.[21] We herein describe the synthesis of the first $[Fe_4S_4]$−alkyl cluster and investigations into how the alkyl ligand perturbs the electronic structure of the $[Fe_4S_4]$ core.

Chart 1. Examples of Proposed $[Fe_4S_4]$−Alkyl Intermediates

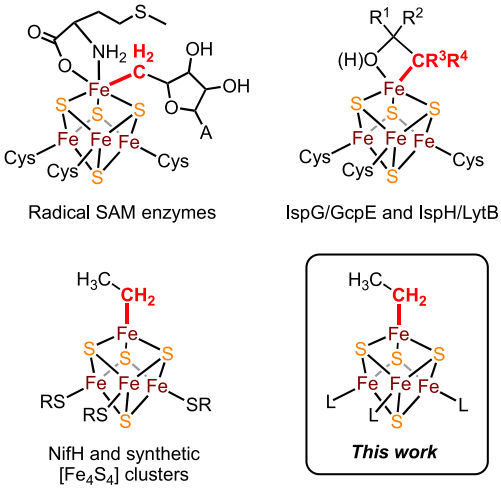

We reasoned that synthetic $[Fe_4S_4]$−alkyl clusters could be accessed by reaction of a nucleophilic alkylating reagent with a 3:1 site-differentiated $[Fe_4S_4]$−halide cluster. This route requires that the clusters be stable and soluble in solvents compatible with alkylating reagents, and we therefore pursued clusters with low overall charge. Inspired by the chelating trithiolate architecture (LS_3) developed by Holm[22,23] and adapted by others,[24,25] we prepared a structurally analogous ligand, $L(N{=}P^{Tol})_3$, featuring three iminophosphorane donors. Iminophosphoranes are strongly basic and, like thiolates, can serve as both σ- and π-donors due to the presence of two lone pairs on the nitrogen atom.[26] In addition, iminophosphoranes are neutral (allowing for compounds with low overall charge and, hence, increased solubility in unreactive solvents), sterically demanding, and tunable at their P-substituents.

The synthesis of $L(N{=}P^{Tol})_3$ (**3**) is shown in Scheme 1. Trianiline **2** was generated via Buchwald−Hartwig coupling

Received: July 1, 2019
Published: August 2, 2019

DOI: 10.1021/jacs.9b06975
J. Am. Chem. Soc. 2019, 141, 13330−13335

Scheme 1. Synthesis of Iminophosphorane-Ligated $[Fe_4S_4]$ Clusters[a]

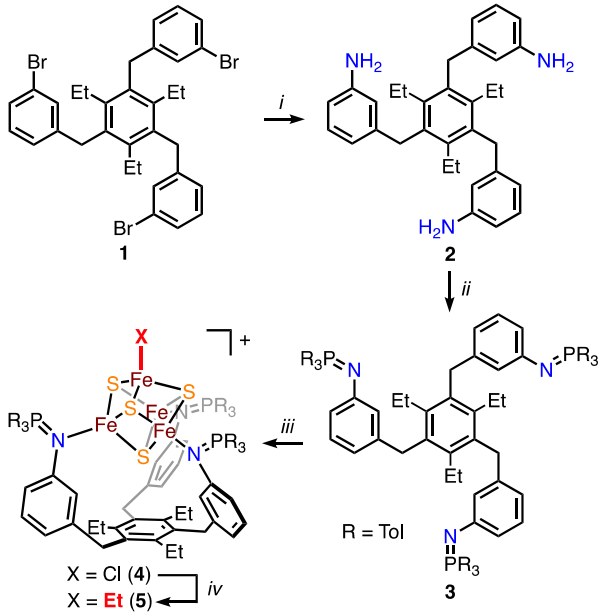

[a]Conditions: (*i*) (a) $Ph_2C{=}NH$ (9 equiv), $Pd_2(dba)_3$ (1.9 mol %), *rac*-BINAP (2.8 mol %), NaO^tBu (10.5 equiv), toluene, 80 °C; (b) 2 M HCl, THF; (c) excess NaOH, MeOH; (*ii*) Tol_3PCl_2 (3 equiv), Et_3N (7 equiv), benzene, 80 °C; (*iii*) $NaBPh_4$ (3 equiv), $[PPh_4]_2[Fe_4S_4Cl_4]$ (1.1 equiv), 1:1 THF/MeCN; (*iv*) Et_2Zn (1.5 equiv), THF.

between tribromide **1** and $Ph_2C{=}NH$ followed by hydrolysis.[27] The iminophosphorane groups were then installed in a Kirsanov reaction using Tol_3PCl_2 and excess Et_3N.

The 3:1 site-differentiated cluster $[(L(N{=}P^{Tol})_3)Fe_4S_4Cl][BPh_4]$ (**4**) can be synthesized on a multigram scale in 65% yield by reaction of $L(N{=}P^{Tol})_3$ with $[PPh_4]_2[Fe_4S_4Cl_4]$ and 3 equiv of $NaBPh_4$ (Scheme 1). The molecular structure of **4** as determined by single-crystal X-ray diffraction (XRD) shows the anticipated 3:1 site differentiation with three Fe atoms bound by $L(N{=}P^{Tol})_3$ and the apical Fe (Fe_{apical}) site bound by Cl (Figure 1a). The molecule has pseudo-C_3 symmetry with one *p*-tolyl group of each iminophosphorane aligned with the pseudo-C_3 axis, forming a protective cavity around the unique Fe site (Figure 1a). The Fe−S distances in **4** are similar to those observed in the 3:1 site-differentiated cluster $[(LS_3)Fe_4S_4Cl]^{2-}$.[23]

Treatment of **4** with Et_2Zn generates the $[Fe_4S_4]$−alkyl complex $[(L(N{=}P^{Tol})_3)Fe_4S_4Et][BPh_4]$ (**5**), which can be isolated as brown solids in 85% yield. The structure of **5** (Figure 1b) was confirmed by single-crystal XRD and is similar to that of **4**. The Fe_{apical}−C bond length of **5** (2.05 Å) is shorter than that in the $[Fe_8S_7]$−decamethylcobaltocenyl cluster (2.12 Å)[21] and comparable to that in a tris(thioether)-borate-ligated Fe^{2+}−Me complex (2.03 Å).[28] In THF solution, **5** slowly decomposes to unidentified products; further reactivity studies of **5** are underway.

The ^{57}Fe Mössbauer spectrum of solid **4** at 90 K (Figure 2a) was simulated as three quadrupole doublets in a 2:1:1 ratio with identical isomer shifts of 0.47 mm/s (Figure 2a, Table 1). This simulation is in accordance with the canonical electronic structure of an $[Fe_4S_4]^{2+}$ cluster: an $S = 0$ ground state arising from antiferromagnetic coupling of two $S = {}^9/_2$ $[Fe_2S_2]^+$ rhombs, each of which consists of spin-aligned, high-spin $Fe^{2.5+}$ ions engaged in a double-exchange interaction.[29] Thus, we assign the doublet comprising 50% of the spectral area to the $[Fe_2S_2]^+$ rhomb bound by two iminophosphorane donors and the second pair of doublets to the Cl-ligated Fe_{apical} center and its spin-aligned, iminophosphorane-ligated partner (Figure 2c). That identical isomer shifts are observed for all sites in this spectrum indicates that each Fe site possesses similar core-charge density, and hence we can assign to each a formal oxidation state (FOS) of 2.5+. Moreover, the similarity between the isomer shifts of **4** and those reported for $[(LS_3)Fe_4S_4Cl]^{2-}$ (δ = 0.46 mm/s at 80 K)[30] and for protein-bound $[Fe_4S_4]^{2+}$ clusters ($\delta \approx 0.42$ mm/s)[31] underscores the utility of the $L(N{=}P^{Tol})_3$ ligand in modeling a trithiolate donor set.

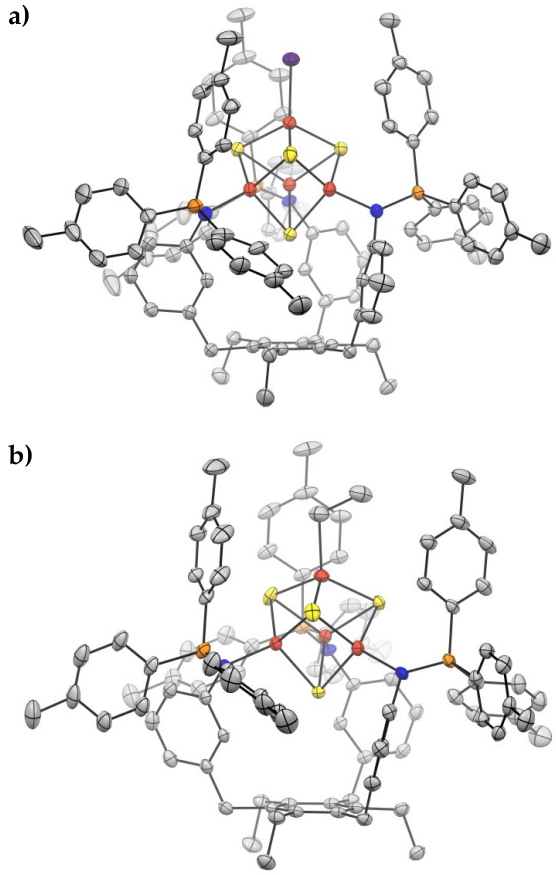

Figure 1. Thermal ellipsoid plots (50%) of (a) **4** and (b) **5**. Hydrogen atoms, solvent molecules, and anions omitted for clarity. Fe (red), S (yellow), Cl (purple), N (blue), P (orange), C (gray).

Complexes **4** and **5** show similar ligand-derived resonances in their room-temperature ^{1}H and ^{31}P NMR spectra. Both exhibit C_3 symmetry in solution as indicated by splitting of the diastereotopic Ar−CH_2−Ar and Ar−CH_2−CH_3 resonances. Their ^{31}P NMR resonances (at 102.1 and 96.0 ppm for **4** and **5**, respectively) are shifted downfield from that of the free ligand **3** (−0.4 ppm), reflecting both the expected downfield shift upon binding a Lewis acidic metal center[32,33] and the population of paramagnetic excited states as is commonly observed in $[Fe_4S_4]^{2+}$ clusters;[23,34−38] their room-temperature solution magnetic moments (μ_{eff} = 2.7 and 2.8 μ_B, respectively) are consistent with this interpretation and typical of $[Fe_4S_4]^{2+}$ clusters.[35,39−41] The ^{1}H NMR signals corresponding to the −CH_3 and −CH_2− protons of the ethyl ligand in **5** are

DOI: 10.1021/jacs.9b06975
J. Am. Chem. Soc. 2019, 141, 13330−13335

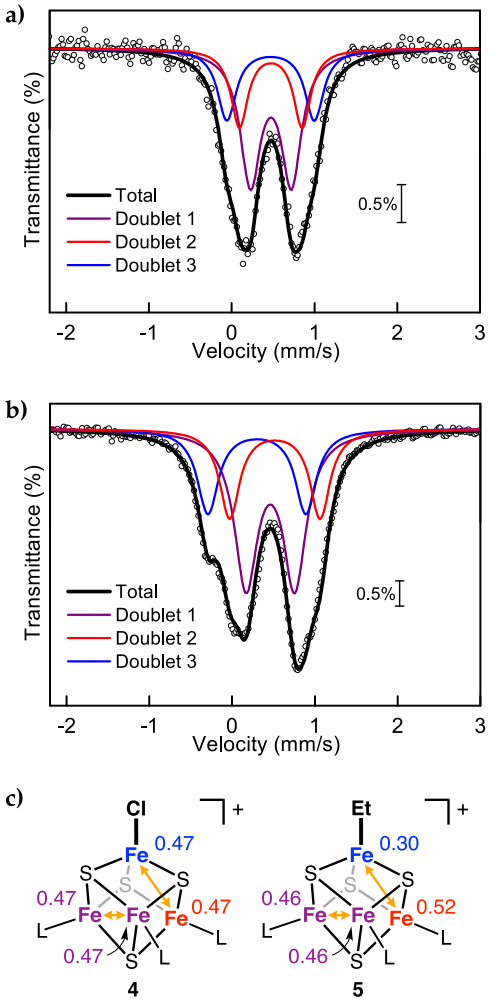

Figure 2. Zero-field ^{57}Fe-Mössbauer spectra of solid (a) **4** and (b) **5** at 90 K. Black circles represent experimental data; solid lines are simulations. (c) Assignments of doublets to individual Fe sites. Isomer shifts indicated in mm/s, and double-exchange interactions indicated by orange arrows.

observed at −4.6 and 70.0 ppm, respectively, which also indicates the population of paramagnetic excited states.[23,34−38] Clusters **4** and **5** exhibit reversible, one-electron reduction events in their cyclic voltammograms at −1.48 and −1.78 V vs Fc/Fc^+, respectively (see Supporting Information (SI)), reflecting the greater electron-donating ability of the ethyl ligand compared with that of the chloride.

As above, the ^{57}Fe Mössbauer spectrum of solid **5** at 90 K (Figure 2b) was simulated with three quadrupole doublets in a 2:1:1 ratio. This approach produces two reasonable models (Table 1); our preferred model (*vide infra*) is shown in Figure 2b,c, and alternatives are discussed in the SI. Both models feature a doublet comprising 50% of the total area with parameters that are nearly identical to those found for the iminophosphorane-bound $Fe^{2.5+}$ sites in **4** (Table 1); this doublet is therefore assigned to the analogous $Fe^{2.5+}$ sites in **5**. The quadrupole doublet with the lowest isomer shift is assigned to the alkylated Fe site because the stronger electron-donating ability (*vide supra*) and increased covalency of the ethyl group relative to $L(N{=}P^{Tol})_3$ are expected to enhance the charge density at the ^{57}Fe nucleus and drive the isomer shift of this site more negative.[42,43] The major difference between these two models is in the magnitude of this effect (δ = 0.30 vs 0.39 mm/s) and whether the remaining iminophosphorane-bound Fe site, which is coupled to the alkylated site via a double-exchange interaction, possesses an isomer shift that is greater or less than that of the other ligand-bound pair (δ = 0.52 vs 0.44 mm/s, compared with 0.46 mm/s for the other ligand-bound pair).

In order to distinguish between these two models, we turned to broken-symmetry density functional theory (BS DFT) calculations (see SI for details). The isomer shifts calculated for **4** (Table 1) are in good agreement with the experimental values. To make the connection between δ and the FOS of the Fe sites, we further analyzed the BS determinants in terms of localized molecular orbitals (LMOs).[44] For each site, the LMOs naturally partition into a set of five spin-up (or down) Fe 3d orbitals, plus an extra spin down (or up) 3d-derived orbital that is delocalized over a single additional Fe site. This picture corresponds to the canonical electronic structure of the $[Fe_4S_4]^{2+}$ cluster[18,19] in which the double-exchange interaction is mediated by the extra delocalized orbital (Figure 3). Through a population analysis, we characterized the tendency of the itinerant electron to localize on either of the two Fe sites engaging in double exchange and thereby assigned FOSs. In the case of **4**, the itinerant electrons are fully delocalized, leading to FOS assignments of ∼2.5+ for each site (Table 1 and Figure 3), consistent with the experimentally observed isomer shifts.

For **5**, the calculated isomer shift of the alkylated site, 0.22 mm/s, is most consistent with the simulated value of 0.30 mm/s. Moreover, the calculation predicts that the isomer shift of the iminophosphorane-bound Fe that is coupled to the alkylated site via double exchange *increases* relative to those of the remaining Fe sites—precisely what is observed in the favored simulation presented in Table 1. While the low isomer shift of the alkylated site might be expected on the basis of the properties of the alkyl ligand (*vide supra*), the compensatory increase in the isomer shift of the spin-aligned Fe is unusual and suggests partial charge localization within this double-exchange-coupled pair. Indeed, the calculated FOS of 2.31+ for

Table 1. Experimental (90 K) and Computed Mössbauer Parameters for 4 and 5

		4 (X = Cl)				**5** (X = Et)					
		Simulation		Calculation		Favored simulation		Disfavored simulation		Calculation	
Doublet	Site	δ (mm/s)	$\lvert\Delta E_Q\rvert$ (mm/s)	δ_{calc}(mm/s)	FOS[a]	δ (mm/s)	$\lvert\Delta E_Q\rvert$ (mm/s)	δ (mm/s)	$\lvert\Delta E_Q\rvert$ (mm/s)	δ_{calc}(mm/s)	FOS[a]
1	Fe−L	0.47	0.48	0.45	2.50+	0.46	0.59	0.46	0.58	0.46	2.58+
				0.46	2.59+					0.47	2.51+
2	Fe−L[b]	0.47	0.75	0.45	2.54+	0.52	1.09	0.44	0.93	0.52	2.31+
3	Fe−X[b]	0.47	1.06	0.50	2.54+	0.30	1.18	0.39	1.36	0.22	2.79+

[a]FOSs are determined from a population analysis of the LMOs of each BS determinant. See SI for details. [b]Sites coupled via double exchange.

DOI: 10.1021/jacs.9b06975
J. Am. Chem. Soc. 2019, 141, 13330−13335

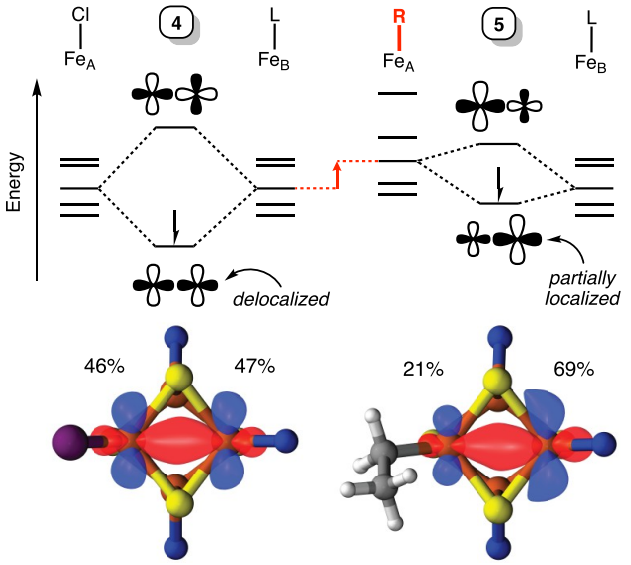

Figure 3. Double-exchange interactions in the β manifold of the $[Fe_2S_2]^+$ rhombs in **4** and **5**. (Top) Molecular orbital diagram showing polarization of the double-exchange interaction upon introduction of an electron-rich alkyl ligand. (Bottom) Isosurface plots (0.05 au) of the double-exchange interaction orbitals with Fe-based Löwdin population analysis.

this site in **5** suggests increased ferrous character, and this charge localization is coupled to an increase in the FOS of the alkylated site to 2.79+ (Table 1).

Physically, this partial charge localization can be understood in terms of localized ligand field effects about the Fe sites engaging in double-exchange delocalization.[17,45] Assuming that double exchange occurs through a single orbital interaction, then two Fe sites with very similar ligand fields will share the itinerant electron equally, producing an effective valence of 2.5+; this appears to be the case, both experimentally and computationally, for all sites in **4** (Figure 3). The symmetry of the double-exchange interaction is removed by alkylation in **5** whereby the electron-releasing alkyl ligand raises the average energy of the local Fe 3d manifold (Figure 3). As a result, the itinerant electron will tend to localize on the site to which the alkylated Fe is coupled, as observed. Similar electronic desymmetrization may alternatively be induced by differences in coordination number between double-exchange-coupled Fe sites.[46] Although a two-orbital model of double exchange is likely too simplistic, these arguments should hold in the case of a more complex multiorbital picture.[18,47]

In conclusion, we have reported the synthesis and characterization of 3:1 site-differentiated $[Fe_4S_4]^{2+}$–Cl and $[Fe_4S_4]^{2+}$–Et clusters that are supported by a chelating triiminophosphorane ligand. NMR and Mössbauer spectroscopic data indicate that, although both clusters have typical diamagnetic ground states, the $[Fe_4S_4]^{2+}$–Et cluster exhibits a polarized Fe–Fe double-exchange interaction, partially localizing ferric character at the alkylated Fe site and ferrous character at its spin-aligned partner. Based on these results, we anticipate that enzymatic $[Fe_4S_4]$–alkyl intermediates may exhibit partial or even complete localization of Fe^{3+} at their alkylated sites. Further investigations into the reactivity of $[Fe_4S_4]^{2+}$–alkyl clusters and efforts to access $[Fe_4S_4]$–alkyl clusters in other redox states and coordination numbers are currently underway in our laboratory.

■ ASSOCIATED CONTENT

Supporting Information

The Supporting Information is available free of charge on the ACS Publications website at DOI: 10.1021/jacs.9b06975.

Experimental procedures, spectra, and computational details (PDF)

Crystallographic data for **4** (CIF)

Crystallographic data for **5** (CIF)

■ AUTHOR INFORMATION

Corresponding Author

*suess@mit.edu

ORCID

Mengshan Ye: 0000-0003-2709-8135

Niklas B. Thompson: 0000-0003-2745-4945

Alexandra C. Brown: 0000-0002-2410-9217

Daniel L. M. Suess: 0000-0002-0916-1973

Notes

The authors declare no competing financial interest.

■ ACKNOWLEDGMENTS

We thank Prof. Theodore Betley (Harvard) for use of his Mössbauer spectrometer, Kevin Anderton (Harvard) for assistance with acquiring Mössbauer data, and Drs. Peter Müller and Charlene Tsay (MIT) for assistance with X-ray crystallographic experiments. This work was supported by the MIT Skoltech Program.

■ REFERENCES

(1) Cammack, R. Iron-Sulfur Clusters in Enzymes: Themes and Variations. *Adv. Inorg. Chem.* **1992**, *38*, 281–322.

(2) Beinert, H.; Holm, R. H.; Münck, E. Iron-Sulfur Clusters: Nature's Modular, Multipurpose Structures. *Science* **1997**, *277*, 653–659.

(3) Rees, D. C.; Howard, J. B. The Interface Between the Biological and Inorganic Worlds: Iron-Sulfur Metalloclusters. *Science* **2003**, *300*, 929–931.

(4) Rouault, T. A. Iron-Sulfur Proteins Hiding in Plain Sight. *Nat. Chem. Biol.* **2015**, *11*, 442–445.

(5) Wang, W.; Li, J.; Wang, K.; Huang, C.; Zhang, Y.; Oldfield, E. Organometallic Mechanism of Action and Inhibition of the 4Fe-4S Isoprenoid Biosynthesis Protein GcpE (IspG). *Proc. Natl. Acad. Sci. U. S. A.* **2010**, *107*, 11189–11193.

(6) Xu, W.; Lees, N. S.; Adedeji, D.; Wiesner, J.; Jomaa, H.; Hoffman, B. M.; Duin, E. C. Paramagnetic Intermediates of (*E*)-4-Hydroxy-3-methylbut-2-enyl Diphosphate Synthase (GcpE/IspG) under Steady-State and Pre-Steady-State Conditions. *J. Am. Chem. Soc.* **2010**, *132*, 14509–14520.

(7) Wang, W.; Wang, K.; Li, J.; Nellutla, S.; Smirnova, T. I.; Oldfield, E. An ENDOR and HYSCORE Investigation of a Reaction Intermediate in IspG (GcpE) Catalysis. *J. Am. Chem. Soc.* **2011**, *133*, 8400–8403.

(8) Xu, W.; Lees, N. S.; Hall, D.; Welideniya, D.; Hoffman, B. M.; Duin, E. C. A Closer Look at the Spectroscopic Properties of Possible Reaction Intermediates in Wild-Type and Mutant (*E*)-4-Hydroxy-3-methylbut-2-enyl Diphosphate Reductase. *Biochemistry* **2012**, *51*, 4835–4849.

(9) Li, J.; Wang, K.; Smirnova, T. I.; Khade, R. L.; Zhang, Y.; Oldfield, E. Isoprenoid Biosynthesis: Ferraoxetane or Allyl Anion Mechanism for IspH Catalysis? *Angew. Chem., Int. Ed.* **2013**, *52*, 6522–6525.

(10) Wang, W.; Oldfield, E. Bioorganometallic Chemistry with IspG and IspH: Structure, Function, and Inhibition of the $[Fe_4S_4]$ Proteins

DOI: 10.1021/jacs.9b06975
J. Am. Chem. Soc. 2019, 141, 13330–13335

Involved in Isoprenoid Biosynthesis. *Angew. Chem., Int. Ed.* **2014**, *53*, 4294−4310.
(11) Cutsail, G. E.; Telser, J.; Hoffman, B. M. Advanced Paramagnetic Resonance Spectroscopies of Iron-Sulfur Proteins: Electron Nuclear Double Resonance (ENDOR) and Electron Spin Echo Envelope Modulation (ESEEM). *Biochim. Biophys. Acta, Mol. Cell Res.* **2015**, *1853*, 1370−1394.
(12) Stiebritz, M. T.; Hiller, C. J.; Sickerman, N. S.; Lee, C. C.; Tanifuji, K.; Ohki, Y.; Hu, Y. Ambient Conversion of CO_2 to Hydrocarbons by Biogenic and Synthetic [Fe_4S_4] Clusters. *Nat. Catal.* **2018**, *1*, 444−451.
(13) Horitani, M.; Shisler, K.; Broderick, W. E.; Hutcheson, R. U.; Duschene, K. S.; Marts, A. R.; Hoffman, B. M.; Broderick, J. B. Radical SAM Catalysis via an Organometallic Intermediate with an Fe-[5′-C]-Deoxyadenosyl Bond. *Science* **2016**, *352*, 822−825.
(14) Dong, M.; Kathiresan, V.; Fenwick, M. K.; Torelli, A. T.; Zhang, Y.; Caranto, J. D.; Dzikovski, B.; Sharma, A.; Lancaster, K. M.; Freed, J. H.; Ealick, S. E.; Hoffman, B. M.; Lin, H. Organometallic and Radical Intermediates Reveal Mechanism of Diphthamide Biosynthesis. *Science* **2018**, *359*, 1247−1250.
(15) Byer, A. S.; Yang, H.; McDaniel, E. C.; Kathiresan, V.; Impano, S.; Pagnier, A.; Watts, H.; Denler, C.; Vagstad, A. L.; Piel, J.; Duschene, K. S.; Shepard, E. M.; Shields, T. P.; Scott, L. G.; Lilla, E. A.; Yokoyama, K.; Broderick, W. E.; Hoffman, B. M.; Broderick, J. B. Paradigm Shift for Radical S-Adenosyl-L-Methionine Reactions: The Organometallic Intermediate Ω Is Central to Catalysis. *J. Am. Chem. Soc.* **2018**, *140*, 8634−8638.
(16) For recent reviews on radical SAM enzymes, see: (a) Broderick, J. B.; Duffus, B. R.; Duschene, K. S.; Shepard, E. M. Radical S-Adenosylmethionine Enzymes. *Chem. Rev.* **2014**, *114*, 4229−4317. (b) Landgraf, B. J.; McCarthy, E. L.; Booker, S. J. Radical S-Adenosylmethionine Enzymes in Human Health and Disease. *Annu. Rev. Biochem.* **2016**, *85*, 485−514. (c) Holliday, G. L.; Akiva, E.; Meng, E. C.; Brown, S. D.; Calhoun, S.; Pieper, U.; Sali, A.; Booker, S. J.; Babbitt, P. C. Atlas of the Radical SAM Superfamily: Divergent Evolution of Function Using a "Plug and Play" Domain. *Methods Enzymol.* **2018**, *606*, 1−71.
(17) Blondin, G.; Girerd, J.-J. Interplay of Electron Exchange and Electron Transfer in Metal Polynuclear Complexes in Proteins or Chemical Models. *Chem. Rev.* **1990**, *90*, 1359−1376.
(18) Noodleman, L.; Peng, C. Y.; Case, D. A.; Mouesca, J.-M. Orbital Interactions, Electron Delocalization and Spin Coupling in Iron-Sulfur Clusters. *Coord. Chem. Rev.* **1995**, *144*, 199−244.
(19) Noodleman, L.; Lovell, T.; Liu, T.; Himo, F.; Torres, R. A. Insights into Properties and Energetics of Iron−Sulfur Proteins from Simple Clusters to Nitrogenase. *Curr. Opin. Chem. Biol.* **2002**, *6*, 259−273.
(20) Thomson, J.; Baird, M. C. Trends in the Spectrochemical Series and ^{31}P Chemical Shifts of Five-Coordinated Cyclopentadienylnickel(II) Complexes. *Can. J. Chem.* **1973**, *51*, 1179−1182.
(21) Ohki, Y.; Murata, A.; Imada, M.; Tatsumi, K. C-H Bond Activation of Decamethylcobaltocene Mediated by a Nitrogenase Fe_8S_7 P-Cluster Model. *Inorg. Chem.* **2009**, *48*, 4271−4273.
(22) Stack, T. D. P.; Holm, R. H. Subsite-Specific Functionalization of the $[4Fe\text{-}4S]^{2+}$ Analog of Iron-Sulfur Protein Clusters. *J. Am. Chem. Soc.* **1987**, *109*, 2546−2547.
(23) Stack, T. D. P.; Holm, R. H. Subsite-Differentiated Analogs of Biological $[4Fe\text{-}4S]^{2+}$ Clusters: Synthesis, Solution and Solid-State Structures, and Subsite-Specific Reactions. *J. Am. Chem. Soc.* **1988**, *110*, 2484−2494.
(24) Walsdorff, C.; Saak, W.; Pohl, S. A New Preorganized Tridentate Ligand Bearing Three Indolethiolate Groups. Preparation of 3:1 Subsite-Differentiated Fe_4S_4 Clusters. *J. Chem. Soc., Dalton Trans.* **1997**, No. 11, 1857−1862.
(25) Terada, T.; Wakimoto, T.; Nakamura, T.; Hirabayashi, K.; Tanaka, K.; Li, J.; Matsumoto, T.; Tatsumi, K. Tridentate Thiolate Ligands: Application to the Synthesis of the Site-Differentiated [4Fe-4S] Cluster Having a Hydrosulfide Ligand at the Unique Iron Center. *Chem. - Asian J.* **2012**, *7*, 920−929.
(26) Cao, T. P. A.; Labouille, S.; Auffrant, A.; Jean, Y.; Le Goff, X. F.; Le Floch, P. Pd(II) and Ni(II) Complexes Featuring a "Phosphasalen" Ligand: Synthesis and DFT Study. *Dalt. Trans.* **2011**, *40*, 10029−10037.
(27) Wolfe, J. P.; Åhman, J.; Sadighi, J. P.; Singer, R. A.; Buchwald, S. L. An Ammonia Equivalent for the Palladium-Catalyzed Amination of Aryl Halides and Triflates. *Tetrahedron Lett.* **1997**, *38*, 6367−6370.
(28) Popescu, C. V.; Mock, M. T.; Stoian, S. A.; Dougherty, W. G.; Yap, G. P. A.; Riordan, C. G. A High-Spin Organometallic Fe−S Compound: Structural and Mössbauer Spectroscopic Studies of [Phenyltris((tert-butylthio)methyl)borate]Fe(Me). *Inorg. Chem.* **2009**, *48*, 8317−8324.
(29) For seminal work on the application of double-exchange in the understanding the electronic structures of Fe−S clusters, see: (a) Noodleman, L.; Baerends, E. J. Electronic Structure, Magnetic Properties, ESR, and Optical Spectra for 2-Fe Ferredoxin Models by LCAO-Xα Valence Bond Theory. *J. Am. Chem. Soc.* **1984**, *106*, 2316−2327. (b) Papaefthymiou, V.; Girerd, J.-J.; Moura, I.; Moura, J. J. G.; Münck, E. Mössbauer Study of *D. gigas* Ferredoxin II and Spin-Coupling Model for the Fe_3S_4 Cluster with Valence Delocalization. *J. Am. Chem. Soc.* **1987**, *109*, 4703−4710. (c) Girerd, J.-J.; Papaefthymiou, V.; Surerus, K. K.; Münck, E. Double Exchange in Iron-sulfur Clusters and a Proposed Spin-dependent transfer mechanism. *Pure Appl. Chem.* **1989**, *61*, 805−816.
(30) Victor, E.; Lippard, S. J. A Tetranitrosyl [4Fe-4S] Cluster Forms En Route to Roussins Black Anion: Nitric Oxide Reactivity of $[Fe_4S_4(LS_3)L']^{2-}$. *Inorg. Chem.* **2014**, *53*, 5311−5320.
(31) Pandelia, M. E.; Lanz, N. D.; Booker, S. J.; Krebs, C. Mössbauer Spectroscopy of Fe/S Proteins. *Biochim. Biophys. Acta, Mol. Cell Res.* **2015**, *1853*, 1395−1405.
(32) Bayram, M.; Gondzik, S.; Bläser, D.; Wölper, C.; Schulz, S. Syntheses and Structures of Zinc Bis(Phosphinimino)Methanide Complexes. *Z. Anorg. Allg. Chem.* **2016**, *642*, 847−852.
(33) Aguilar, D.; Navarro, R.; Soler, T.; Urriolabeitia, E. P. Regioselective Functionalization of Iminophosphoranes through Pd-Mediated C−H Bond Activation: C−C and C−X Bond Formation. *Dalt. Trans.* **2010**, *39*, 10422−10431.
(34) Holm, R. H.; Phillips, W. D.; Averill, B. A.; Mayerle, J. J.; Herskovitz, T. Synthetic Analogs of the Active Sites of Iron-Sulfur Proteins. V. Proton Resonance Properties of the Tetranuclear Clusters $[Fe_4S_4(SR)_4]^{2-}$. *J. Am. Chem. Soc.* **1974**, *96*, 2109−2117.
(35) Papaefthymiou, G. C.; Laskowski, E. J.; Frota-Pessoa, S.; Frankel, R. B.; Holm, R. H. Antiferromagnetic Exchange Interactions in $[Fe_4S_4(SR)_4]^{2-,3-}$ Clusters. *Inorg. Chem.* **1982**, *21*, 1723−1728.
(36) Weigel, J. A.; Holm, R. H. Intrinsic Binding Properties of a Differentiated Iron Subsite in Analogues of Native $[Fe_4S_4]^{2+}$ Clusters. *J. Am. Chem. Soc.* **1991**, *113*, 4184−4191.
(37) Zhou, C.; Holm, R. H. Comparative Isotropic Shifts, Redox Potentials, and Ligand Binding Propensities of [1:3] Site-Differentiated Cubane-Type $[Fe_4Q_4]^{2+}$ Clusters (Q = S, Se). *Inorg. Chem.* **1997**, *36*, 4066−4077.
(38) Hoveyda, H. R.; Holm, R. H. Characterization of the Self-Condensation Equilibrium of $[Fe_4S_4(SH)_4]^{2-}$: Spectroscopic Identification of a Unique Sulfido-Bridged Acyclic Tricubane Cluster. *Inorg. Chem.* **1997**, *36*, 4571−4578.
(39) Wong, G. B.; Bobrik, M. A.; Holm, R. H. Inorganic Derivatives of Iron Sulfide Thiolate Dimers and Tetramers: Synthesis and Properties of the Halide Series $[Fe_2S_2X_4]^{2-}$ and $[Fe_4S_4X_4]^{2-}$ (X = Chlorine, Bromine, Iodine). *Inorg. Chem.* **1978**, *17*, 578−584.
(40) Laskowski, E. J.; Frankel, R. B.; Gillum, W. O.; Papaefthymiou, G. C.; Renaud, J.; Ibers, J. A.; Holm, R. H. Synthetic Analogs of the 4-Fe Active Sites of Reduced Ferredoxins. Electronic Properties of the Tetranuclear Trianions $[Fe_4S_4(SR)_4]^{3-}$ and the Structure of $[(C_2H_5)_3(CH_3)N]_3[Fe_4S_4(SC_6H_5)_4]$. *J. Am. Chem. Soc.* **1978**, *100*, 5322−5337.
(41) McSkimming, A.; Suess, D. L. M. Selective Synthesis of Site-Differentiated Fe_4S_4 and Fe_6S_6 Clusters. *Inorg. Chem.* **2018**, *57*, 14904−14912.

DOI: 10.1021/jacs.9b06975
J. Am. Chem. Soc. 2019, 141, 13330−13335

(42) The isomer shifts of isostructural, high-spin Fe^{2+}−Cl (δ = 0.74 mm/s) and −Me (δ = 0.48 mm/s) complexes show a similar trend in which the alkylated site exhibits a lower isomer shift. See: Andres, H.; Bominaar, E. L.; Smith, J. M.; Eckert, N. A.; Holland, P. L.; Münck, E. Planar Three-Coordinate High-Spin Fe^{II} Complexes with Large Orbital Angular Momentum: Mössbauer, Electron Paramagnetic Resonance, and Electronic Structure Studies. *J. Am. Chem. Soc.* **2002**, *124*, 3012−3025.

(43) Neese, F.; Petrenko, T. Quantum Chemistry and Mössbauer Spectroscopy. In *Mössbauer Spectroscopy and Transition Metal Chemistry. Fundamentals and Applications*; Gutlich, P., Bill, E., Trautwein, A. X., Eds.; Springer-Verlag Berlin Heidelberg: New York, 2011; pp 137−199.

(44) Bjornsson, R.; Neese, F.; DeBeer, S. Revisiting the Mössbauer Isomer Shifts of the FeMoco Cluster of Nitrogenase and the Cofactor Charge. *Inorg. Chem.* **2017**, *56*, 1470−1477.

(45) Noodleman, L.; Case, D. A.; Mouesca, J.-M.; Lamotte, B. Valence Electron Delocalization in Polynuclear Iron-Sulfur Clusters. *J. Biol. Inorg. Chem.* **1996**, *1*, 177−182.

(46) Ciurli, S.; Carrie, M.; Weigel, J. A.; Carney, M. J.; Stack, T. D. P.; Papaefthymiou, G. C.; Holm, R. H. Subsite-Differentiated Analogs of Native Iron Sulfide $[4Fe\text{-}4S]^{2+}$ Clusters: Preparation of Clusters with Five- and Six-Coordinate Subsites and Modulation of Redox Potentials and Charge Distributions. *J. Am. Chem. Soc.* **1990**, *112*, 2654−2664.

(47) Sharma, S.; Sivalingam, K.; Neese, F.; Chan, G. K. L. Low-Energy Spectrum of Iron-Sulfur Clusters Directly from Many-Particle Quantum Mechanics. *Nat. Chem.* **2014**, *6*, 927−933.

DOI: 10.1021/jacs.9b06975
J. Am. Chem. Soc. 2019, 141, 13330−13335